Role of saddle-to-scission dynamics in fission fragment mass distribution

Jhilam Sadhukhan[*] and Santanu Pal[†]

Physics Group, Variable Energy Cyclotron Centre, 1/AF Bidhan Nagar, Kolkata 700 064, India

The fragment mass distribution from fission of hot nuclei is studied in the framework of two-dimensional Langevin equations. The mass asymmetry coordinate distribution is obtained from the dynamical calculation both at the saddle and the scission regions in order to investigate the role of saddle-to-scission dynamics in fission fragment mass distribution. Statistical model predictions of mass asymmetry distributions at saddle and scission are also compared with the dynamical model results. Results for a number of nuclei covering a broad range of saddle-to-scission distances are presented.

PACS number(s): 25.85.Ge, 05.10.Gg, 05.40.Jc, 24.10.Pa

I. INTRODUCTION

Nuclear fission is a unique process in which the shape of a nearly equilibrated system evolves continuously till it splits into two fragments. The probability of finding a compound nucleus (CN) separating into fragments with given masses depends upon both the statistical and the dynamical properties of the fissioning system. Fong [1] first developed a statistical theory for the fission fragment mass distribution where it was assumed that a complete equilibration among all the degrees of freedom is established in the fissioning nucleus at every instant and the relative probability of a given mass partition is proportional to the density of quantum states at the scission point. The statistical theory successfully explained the mass yield in thermal-neutron-induced fission. Nix and Swiatecki [2] subsequently pointed out that the saddle configuration is a better static point than the scission one since the latter cannot be defined in a unique manner. They assumed an equilibrated distribution at the saddle configuration and the transition from the saddle to the scission was treated dynamically without considering any dissipation. This approach gave a reasonable agreement with experimentally measured fission fragment mass variances for α-particle-induced fission of CN up to mass number $A = 213$ [3]. A dissipative force was subsequently included in the saddle-to-scission motion [4,5]. In order to explain the mass variances observed in the fission of heavier CN, the importance of stochastic dynamics during the saddle-to-scission transition was later established by Adeev and Pashkevich [6]. In recent years, fission fragment mass and kinetic energy distributions have been calculated by several authors from full stochastic dynamical treatments of the evolution of a hot CN from ground state to scission configuration [7–15].

A suitable model to describe the stochastic dynamics of a hot compound nucleus is that of a Brownian particle in a heat bath. In this model, the collective motion involving the fission degrees of freedom is represented by a Brownian particle while the remaining intrinsic degrees of freedom of the CN correspond to the heat bath. In addition to the random force experienced by the Brownian particle in the heat bath, its motion is also controlled by the average nuclear potential. Fission occurs when the Brownian particle picks up sufficient kinetic energy from the heat bath in order to overcome the fission barrier. The dynamics of such a system is dissipative in nature and is governed by the appropriate Langevin equations or equivalently by the corresponding Fokker-Planck equation. An analytical solution for the stationary diffusion rate of Brownian particles across the barrier was first obtained by Kramers from the Fokker-Planck equation [16]. The Fokker-Planck equation was subsequently used for extensive studies of nuclear fission [17–26]. The Langevin equations however found wider applications in recent years mainly because, unlike the Fokker-Planck equation, the Langevin equations do not require any approximation and it is easier to solve the latter for multidimensional cases by numerical simulations [27]. Fairly successful Langevin dynamical calculations for several observables such as fission and evaporation residue cross sections, pre-scission multiplicities of light particles and giant dipole resonance γ rays, and mass and kinetic energy distributions of the fission fragments have been reported [7–15,28–42].

In a stochastic dynamical model of nuclear fission, the fission fragment mass distribution essentially portrays the interplay between the conservative and the random forces acting along the mass asymmetry coordinate. Therefore, it will be of interest to find how the fluctuation in the mass asymmetry coordinate changes as the CN makes its journey from the saddle region to the scission configuration. This will essentially involve comparison of the asymmetry coordinate distribution at the saddle with that at the scission configuration. Such a comparison is expected to elucidate the role of the potential landscape vis-à-vis that of the random force in giving rise to the fission fragment mass distribution at scission [7,9,10]. The "memory" of the asymmetry coordinate fluctuation at the saddle that is retained at scission has also been discussed earlier on several occasions [6,12]. We address the above issues in the present work.

The fragment mass dispersions at the saddle and scission were compared in an earlier work of Gontchar *et al.* [9], where the mass variances at the saddle and scission were obtained from statistical and dynamical models, respectively. Though

[*]jhilam@vecc.gov.in

[†]santanu@vecc.gov.in

the mass variance at scission has been obtained from dynamical model calculations by a number of workers [8,9,42] in the past, the mass variance at the saddle has not been calculated from dynamical models so far. In the present calculation we obtain mass variances at both the saddle and scission from dynamical calculation since it is appropriate that both variances be obtained from the same model in order to compare them and investigate effects due to saddle-to-scission transition. In a Langevin dynamical calculation, a fission trajectory crosses the saddle ridge many times in a to-and-fro motion before it reaches the scission line. We obtain the mass asymmetry distribution along the saddle ridge by considering only those mass asymmetries which correspond to the last crossing of the saddle ridge by fission trajectories. The nature of the fission trajectories in the saddle region is further illustrated in the present work by comparing the distributions of the asymmetry coordinates corresponding to the first and last crossings of the saddle ridge by the fission trajectories.

The plan of our work is as follows. We perform Langevin dynamical calculations for fission in two dimensions using elongation and asymmetry as the relevant coordinates. We restrict the present calculation to the above two coordinates primarily because, while they bring out the essential features of the dynamics of the asymmetry coordinate, they also provide easy visualization of the fission process. For each fissioning Langevin trajectory, the asymmetry coordinates at which the trajectory crosses the saddle (for the last time) and scission regions are recorded. We thus directly obtain the asymmetry coordinate distributions at both the saddle and the scission. We make a detailed comparison of these two distributions for different nuclei representing a broad range of distances between the saddle and the scission regions.

We describe the Langevin equations and the various inputs in the next section. The numerical results are presented in Sec. III. The last section contains a summary of the work and a discussion.

II. THE LANGEVIN EQUATIONS AND THE INPUTS

In order to specify the collective coordinates for a dynamical description of nuclear fission, we use the shape parameters (c, h, α') from Ref. [10], where c denotes the elongation parameter, h represents the neck degree of freedom, and the mass asymmetry parameter α' determines the ratio of the volumes (masses) of the future fragments. With the above parameters, the surface of the nucleus in cylindrical coordinates is given as

$$
\rho^2(z) = \left(1 - \frac{z^2}{c^2}\right)\left(a_0 c^2 + b_0 z^2 + \frac{\alpha' z}{c^2}\right), \quad b_0 \geqslant 0,
$$
$$
= \left(1 - \frac{z^2}{c^2}\right)\left[a_0 c^2 + \frac{\alpha' z}{c^2} \exp\left(\frac{b_0 c z^2}{R_0^3}\right)\right], \quad b_0 < 0,
$$
(1)

where

$$
b_0 = 2h + \frac{c - 1}{2}
$$

and

$$
a_0 = \frac{1}{c^3} - \frac{b_0}{5}, \quad b_0 \geqslant 0,
$$
$$
= -\frac{4}{3}\frac{b_0}{e^p + \left(1 + \frac{1}{2p}\right)\sqrt{-\pi p}\,\mathrm{erf}(\sqrt{-p})}, \quad b_0 < 0, \quad (2)
$$

where $p = b_0 c^3$ and erf(x) is the error function. In Eqs. (1) and (2), the parameter h describes the variation of the thickness of the neck without changing the length $2c$ (in units of R_0, the radius of the spherical nuclear radius) of the nucleus along the symmetry axis. Since we do not consider neck dynamics in the present work, we set $h = 0$ in the above equations. The mass asymmetry parameter α' is related to the ratio of the masses (volumes) of the nascent fragments as [10]

$$
\frac{A_1}{A_2} = \frac{V_1}{V_2} = \frac{1 + \frac{3}{8}\alpha'}{1 - \frac{3}{8}\alpha'},
$$

where the masses A_1 and A_2 are the two parts of the nucleus obtained by its intersection with the plane $z = 0$.

The two-dimensional Langevin equation in (c, α') coordinates has the following form [43]:

$$
\frac{dp_i}{dt} = -\frac{p_j p_k}{2}\frac{\partial}{\partial q_i}(m^{-1})_{jk} - \frac{\partial U}{\partial q_i} - \gamma_{ij}(m^{-1})_{jk}p_k + g_{ij}\Gamma_j(t),
$$
(3)
$$
\frac{dq_i}{dt} = (m^{-1})_{ij}p_j,
$$

where q_1 and q_2 stand for c and α', respectively, and p_i represents the respective momentum. U is the potential energy of the system and m_{ij} and γ_{ij} are the shape-dependent collective inertia and dissipation tensors, respectively. The time-correlation property of the random force is assumed to follow the relation

$$
\langle \Gamma_k(t)\Gamma_l(t')\rangle = 2\delta_{kl}\delta(t - t'),
$$

and the strength of the random force is related to the dissipation coefficients through the fluctuation-dissipation theorem and is given as

$$
g_{ik}g_{jk} = \gamma_{ij}T,
$$

where the temperature T of the compound nucleus at any instant of its evolution is given as

$$
T = \sqrt{E_{\mathrm{int}}/a(q)}.
$$

The intrinsic excitation energy E_{int} is calculated from the total excitation energy E^* of the compound nucleus using energy conservation,

$$
E^* = E_{\mathrm{int}} + E_{\mathrm{coll}} + U(q),
$$

where E_{coll} is the collective translational kinetic energy and $U(q)$ is the potential energy including the rotational energy of the system. The level density parameter $a(q)$ depends on the collective coordinates and is taken from the works of Ignatyuk *et al.* [44].

We make the Werner-Wheeler approximation [45] for incompressible irrotational flow to calculate the collective inertia tensor and its inverse $(m^{-1})_{ij}$ in Eq. (3). The potential energy $U(c, \alpha')$ is obtained from the finite-range liquid-drop model by a double folding procedure [46]. The rotational

energy part of $U(c, \alpha')$ is calculated using the moment of inertia of a rigid rotator. For γ_{ij}, we use the one-body model for nuclear dissipation in our calculations. The original wall-plus-window formula [47,48], which was subsequently generalized to include the dissipation associated with the time

rate of change of mass asymmetry degree of freedom [49], is employed here and is given as [10]

$$\gamma_{ij} = \kappa \gamma_{ij}^{\text{wall}} + \gamma_{ij}^{\text{window}} + \gamma_{ij}^{\text{asym}}, \quad (4)$$

where

$$\gamma_{ij}^{\text{wall}} = \frac{1}{2}\pi \rho_m \bar{v} \left\{ \int_{z_{\min}}^{z_N} \left(\frac{\partial \rho^2}{\partial q_i} + \frac{\partial \rho^2}{\partial z}\frac{\partial D_1}{\partial q_i} \right)\left(\frac{\partial \rho^2}{\partial q_j} + \frac{\partial \rho^2}{\partial z}\frac{\partial D_1}{\partial q_j} \right)\left(\rho^2 + \left(\frac{1}{2}\frac{\partial \rho^2}{\partial z} \right)^2 \right)^{-\frac{1}{2}} dz \right.$$
$$\left. + \int_{z_N}^{z_{\max}} \left(\frac{\partial \rho^2}{\partial q_i} + \frac{\partial \rho^2}{\partial z}\frac{\partial D_2}{\partial q_i} \right)\left(\frac{\partial \rho^2}{\partial q_j} + \frac{\partial \rho^2}{\partial z}\frac{\partial D_2}{\partial q_j} \right)\left[\rho^2 + \left(\frac{1}{2}\frac{\partial \rho^2}{\partial z} \right)^2 \right]^{-\frac{1}{2}} dz \right\}, \quad (5)$$

$$\gamma_{ij}^{\text{window}} = \frac{1}{2}\rho_m \bar{v}\frac{\partial R}{\partial q_i}\frac{\partial R}{\partial q_j}\Delta\sigma, \quad (6)$$

and

$$\gamma_{ij}^{\text{asym}} = \frac{16}{9}\rho_m \bar{v}\frac{1}{\Delta\sigma}\frac{\partial V_1}{\partial q_i}\frac{\partial V_1}{\partial q_j}. \quad (7)$$

$\gamma_{ij}^{\text{wall}}$ and $\gamma_{ij}^{\text{window}}$ in the above equations represent the wall and window dissipation coefficients, respectively [48]. It has been established from earlier studies [10] that a smaller strength of the wall dissipation than that given by Eq. (5) is required in order to fit experimental data. κ represents the reduction factor for wall dissipation coefficient in Eq. (4) and a value of $\kappa = 0.25$ is used in the present work [10,14,42]. The coefficient for dissipative resistance against change in asymmetry degree of freedom is given by $\gamma_{ij}^{\text{asym}}$ [49]. This component of one-body dissipation strongly influences the fission fragment mass distribution, as we shall see in the next section. In the above equations, ρ_m and $\bar{v}$ represent the average nuclear mass density and the average nucleon speed within the nucleus, respectively. $\Delta\sigma$ denotes the window area between the two parts of the system while D_1 and D_2 are the positions of the centers of mass of the two parts of the fissioning system relative to the center of mass of the whole system and R is the separation between D_1 and D_2. The two extreme ends of the nuclear shape along the z axis are $z_{\min}$ and $z_{\max}$, and z_N is the position where neck formation begins.

It is of interest at this point to examine the two-dimensional landscapes of various input quantities in our calculation. We first show the potential energy contours in Fig. 1 for six rotating nuclei. The loci of the conditional saddle points or the saddle ridge and that of the scission configurations (scission line) are also shown in this figure for each nuclei. The scission configuration is determined following the criterion given in Ref. [10] and corresponds to a neck radius of $0.3R_0$. The above nuclei and their spin values are so chosen that they represent a broad range of saddle-to-scission distances and also a reasonable range of fission barriers where Langevin dynamical calculations with good statistics can be performed. Table I gives the values of Z^2/A, the distance (c_{SS} in units of R_0) between the saddle ridge and the scission line along the c axis for $\alpha' = 0$, and the fission barrier of these nuclei. We next show in Fig. 1 the locus of the points (neck line) where

neck formation begins in (c, α') space. It is observed that while the saddle-to-scission transition is made through shapes with well-developed necks for lighter nuclei, a large fraction of the transition takes place in heavier nuclei before a neck is formed. Since the component of the stochastic force associated with the mass asymmetry degree of freedom becomes effective after the neck is formed, the above observation indicates that the relative roles of the conservative and stochastic forces are expected to be different for light and heavy nuclei. This aspect will be further explored in the next section.

We next show the contour plots of inverse inertia tensor components of ^{224}Th in Fig. 2. We observe that both the diagonal components $(m^{-1})_{cc}$ and $(m^{-1})_{\alpha'\alpha'}$ have very weak α' dependence though their c dependence is quite strong. The nondiagonal component $(m^{-1})_{c\alpha'}$ however has a stronger α' dependence and a weaker c dependence. This means that the contributions of the diagonal terms in the inertia derivative term in the Langevin equations [Eq. (3)] is much stronger in the c coordinate than that in the α' coordinate while it is the opposite for the nondiagonal term. It is also of interest to note that while the diagonal components $(m^{-1})_{cc}$ and $(m^{-1})_{\alpha'\alpha'}$ have a symmetric α' dependence, it is antisymmetric for the nondiagonal component $(m^{-1})_{c\alpha'}$. The contour plots of the dissipation tensor shown in Fig. 3 also have features similar to those of inertia. The diagonal components are symmetric in α' though they have a somewhat stronger α' dependence compared to inverse inertia. The nondiagonal component $\gamma_{c\alpha'}$ has a strong α' dependence and it is also antisymmetric in α'. The symmetry properties with respect to α' of the inverse inertia and the dissipation coordinates taken together give rise to the correct symmetry of the Langevin dynamical

TABLE I. Z^2/A, saddle-to-scission distance (c_{SS} in units of R_0) and fission barrier (V_B) for symmetric fission of compound nuclei used in the work.

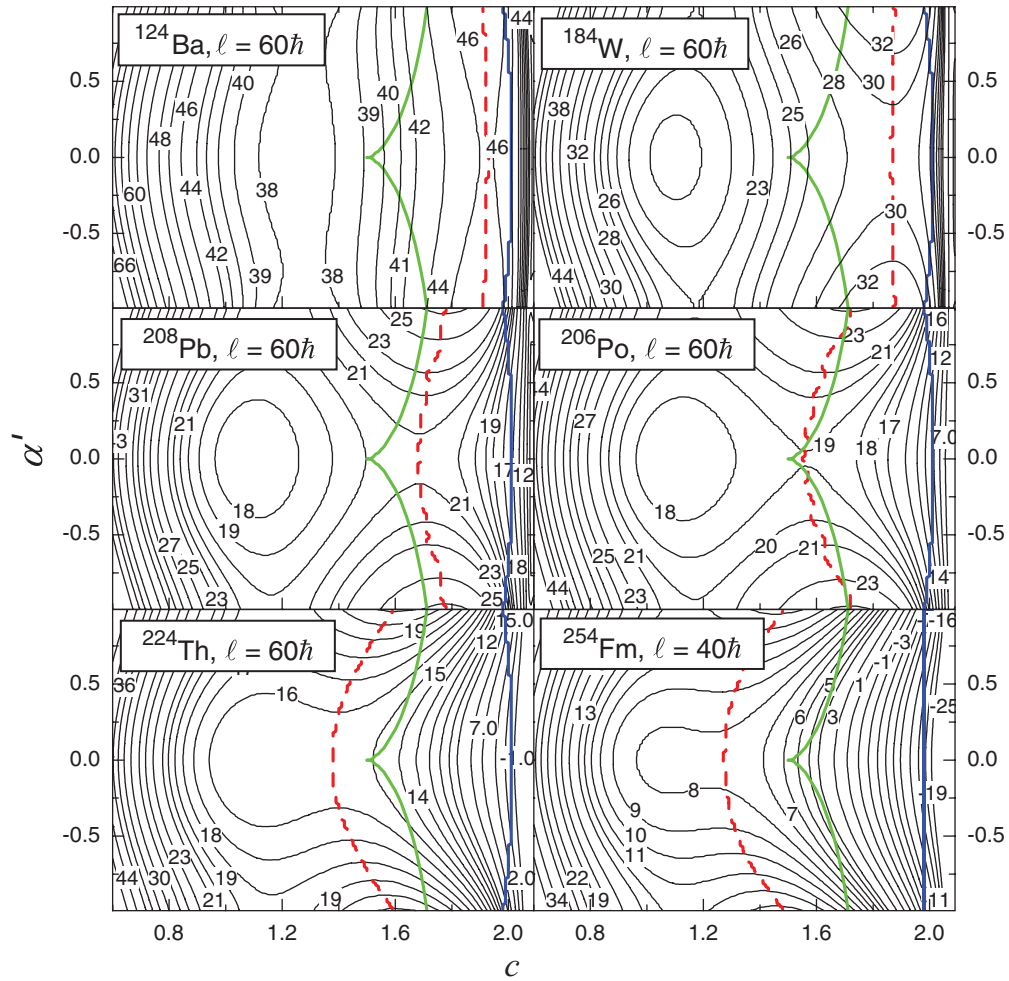|	^{124}Ba $l = 60\hbar$	^{184}W $l = 60\hbar$	^{208}Pb $l = 60\hbar$	^{206}Po $l = 60\hbar$	^{224}Th $l = 60\hbar$	^{254}Fm $l = 40\hbar$
Z^2/A	25.29	29.76	32.33	34.25	36.16	39.37
c_{SS}	0.08	0.14	0.32	0.46	0.63	0.74
V_B (MeV)	8.61	8.63	3.41	1.76	0.38	0.10

FIG. 1. (Color online) The finite-range liquid-drop-model potential contours (in MeV) for a number of compound nuclei. The saddle ridge and scission line are shown by thick dashed and full lines, respectively. The thin gray line represents the neck line (see text).

equations. This essentially implies that the c component of force at c for $(\alpha', p_{\alpha'})$ is the same as that for $(-\alpha', -p_{\alpha'})$. However, the α' component of the force should change sign between $(\alpha', p_{\alpha'})$ and $(-\alpha', -p_{\alpha'})$. Both are realized when diagonal components are symmetric and nondiagonal components antisymmetric with respect to reflection of α'. We also compare the magnitudes of γ_{cc} and $\gamma_{\alpha'\alpha'}$ in Fig. 4. $\gamma_{\alpha'\alpha'}$ is much weaker than γ_{cc} for most values of the elongation parameter c except at large deformations, where a neck has developed, due to the γ^{asym} term.

With the input quantities defined as in the above, the Langevin equations are numerically integrated in second order using a small time step of $0.0005\,\hbar/\mathrm{MeV}$. All the input quantities are first calculated on a uniform two-dimensional grid with 150×101 grid points covering the range of $c \in (0.6, 2.09)$ and $\alpha' \in (-1, 1)$. Calculations are performed for a compound nucleus at specified values of its spin and temperature. The initial collective coordinates are chosen as those of a spherical nucleus and the initial momentum distribution is assumed to follow that of a equilibrated thermal system. In the present calculation, we record the asymmetry coordinate of the crossing point whenever a Langevin trajectory crosses the saddle ridge.

If the same trajectory subsequently reaches the scission line, it is identified as a fission event and the asymmetry coordinate at scission is also recorded. While the asymmetry coordinates corresponding to the last crossing of the saddle ridge by the fission trajectories are used to obtain the mass variance at the saddle, those corresponding to the crossing of the scission line give the mass variance at scission. The fission fragment mass distribution at the saddle thus corresponds to the distribution that would result if the asymmetry distribution at the saddle were transported to the scission configuration without any further modification. The calculations are performed for a large ensemble of Langevin trajectories such that the number of fission events are typically 10 000 or more. Numerical integration of the Langevin equations for each trajectory is continued for a sufficiently long time interval such that a steady flow of fission trajectories across the saddle ridge is established. The fragment mass distributions at saddle and scission configurations are subsequently obtained from the asymmetry coordinate distributions by binning over the asymmetry coordinate. The fragment mass distributions at the saddle and scission are thus obtained from the same set of fission events.
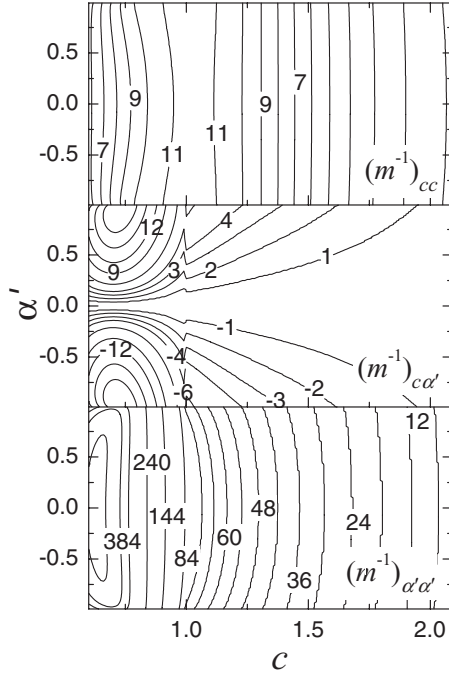
FIG. 2. Different components of the inverse inertia tensor (in MeV/$\hbar^2$) of ^{224}Th.

III. MASS DISPERSION DURING TRANSITION FROM SADDLE RIDGE TO SCISSION LINE

We first show in Fig. 5 the fission fragment mass distributions calculated for nuclei listed in Table I and at a temperature of 2 MeV. This temperature defines the initial excitation energy of a nucleus in its ground-state configuration.
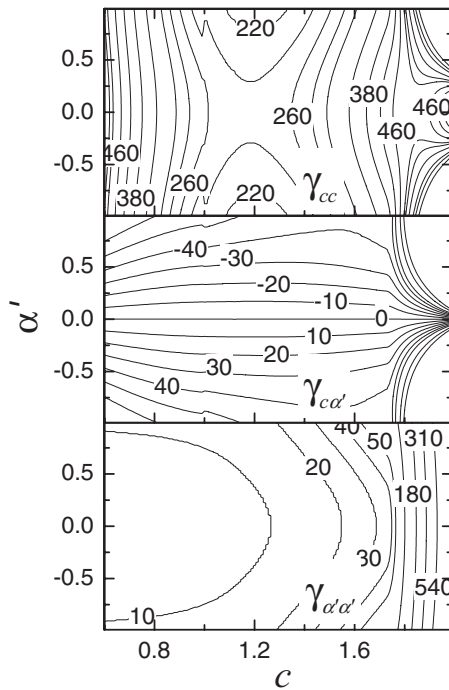

FIG. 3. Different components of one-body dissipation tensor (in units of $\hbar$) calculated for ^{224}Th using Eq. (4) with $\kappa = 0.25$.

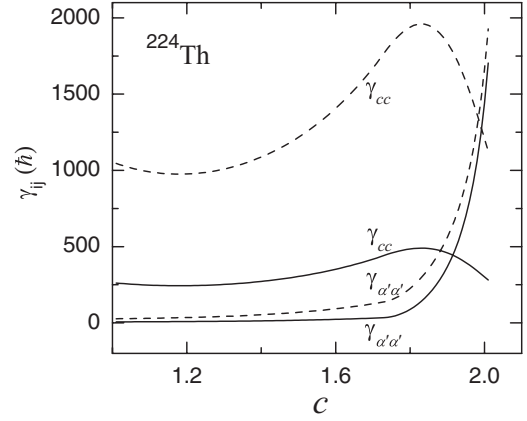FIG. 4. The diagonal components of one-body dissipation plotted against c for $\alpha' = 0$. The solid and dashed lines correspond to different dissipation strengths calculated with $\kappa = 0.25$ and 1, respectively.

The fragment mass distributions calculated at both saddle and scission configurations with the $\gamma^{\rm asym}$ term in Eq. (4) are shown in this figure. Similar calculations are also performed without $\gamma^{\rm asym}$ and the corresponding mean-square deviations σ_m^2 for the different systems are plotted as a function of saddle-to-scission distances c_{SS} in Fig. 6. This figure provides a direct comparison between mass variances at saddle and scission when both are obtained from Langevin dynamical model calculation, in contrast with the results of [9], where the mass variances at saddle and scission were obtained from statistical and dynamical models, respectively. We find that the mass variance of a system decreases as it moves from the saddle to the scission region. Though the magnitude of reduction is very small for small values of c_{SS}, it increases with increasing saddle-to-scission distance. This feature clearly demonstrates the role of the potential landscape in developing the mass variance during saddle-to-scission transition. Since $\gamma^{\rm asym}$ is not included in the calculation of mass variances in Fig. 6, a strong dissipative force is not present in the saddle-to-scission dynamics. Therefore, the funnel shape of the potential landscape in the saddle-to-scission region pushes the system toward a symmetric configuration and consequently the mass variance at scission decreases.

Mass variances obtained with $\gamma^{\rm asym}$ in the Langevin dynamical calculation are next shown in Fig. 7. Dynamical model results without $\gamma^{\rm asym}$ (as given in Fig. 6) are also shown in this figure for comparison. The variances at the saddle obtained with and without $\gamma^{\rm asym}$ are indistinguishable in this figure, which is expected since $\gamma^{\rm asym}$ becomes effective only beyond the neck line. We make two observations from this figure. First, the variances at scission are enhanced (with respect to values obtained without $\gamma^{\rm asym}$) with inclusion of $\gamma^{\rm asym}$ in the calculation. This is a consequence of the random force associated with $\gamma^{\rm asym}$, which operates between the neck line and the scission line and drives the system toward larger asymmetry. This also demonstrates the importance of the asymmetry term $\gamma^{\rm asym}$ in the generalized one-body dissipation [49]. Our next observation concerns a comparison of variances at saddle and scission when both are obtained with the $\gamma^{\rm asym}$ term in the calculation. The variance at scission is found to be
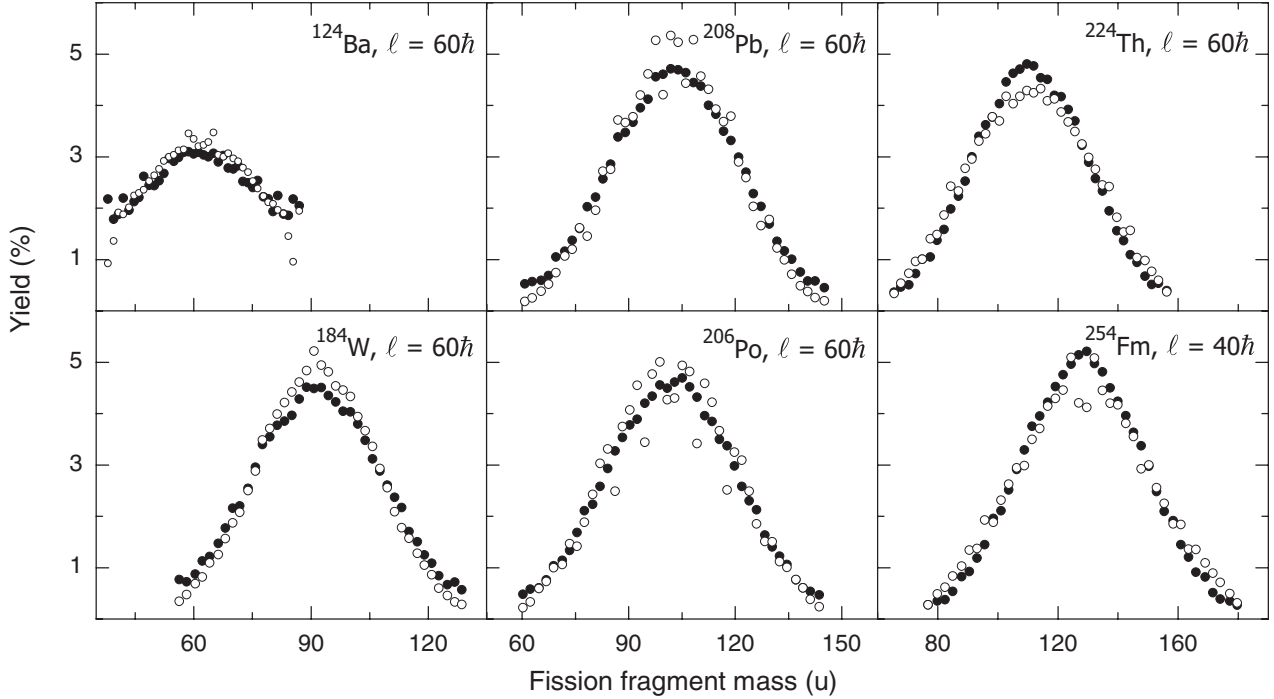
FIG. 5. Fission fragment mass distributions (filled circles) at the scission line for different nuclei obtained from dynamical model calculations with the γ^{asym} term. The mass distributions on the saddle ridge, contributed by the trajectories which eventually reach the scission line, are shown by the empty circles.

larger than that at the saddle for smaller values of c_{SS} while the reverse is the case for higher values of c_{SS}. In order to make a qualitative understanding of this observation, we proceed as follows. From the potential landscape of the different systems given in Fig. 1, we have observed in the earlier section that necks are already developed in the saddle-to-scission region for lighter nuclei (small c_{SS}) while a neck is formed only during the latter stage of saddle-to-scission transition in heavier nuclei (large c_{SS}). Therefore, the random force due to γ^{asym} operates over the entire stretch of the saddle-to-scission region for lighter nuclei while it is effective only for a part of the saddle-to-scission region for heavier nuclei. On the other hand, the funneling effect of the potential landscape is present for all nuclei over the entire saddle-to-scission region. The above scenario suggests that the net effect in driving a system to higher asymmetry as it evolves from saddle-to-scission will be higher for lighter nuclei than for heavier ones. In fact, comparison of mass variances at saddle and scission in Fig. 7 shows that while the mass dispersion grows during saddle-to-scission transition for lighter nuclei, it shrinks for heavier nuclei. It may be pointed out here that the first observation in the above, namely, the reduction of mass variance at scission when γ^{asym} is not included in the calculation, was also made in Ref. [9]. In the present work, we are able to make further observations regarding the changes in mass variances during saddle-to-scission transition since the variances at both saddle and scission are obtained from dynamical calculations.

We have considered different compound nuclei in the above in order to study the effect of saddle-to-scission dynamics in fission fragment mass distributions over a broad range of

saddle-to-scission distances. The saddle-to-scission distance also varies with spin for a given nucleus though over a limited range. The effects are still discernible, as shown in Fig. 8, where fission fragment mass variances of ^{224}Th calculated at three different spin values are shown. The mass variances at saddle and scission are found to depend upon c_{SS} in a manner similar to that obtained while considering a set of different compound nuclei.

The stochastic nature of fission dynamics causes a fission trajectory to cross the saddle ridge a number of times in a to-and-fro motion before it reaches the scission line. In
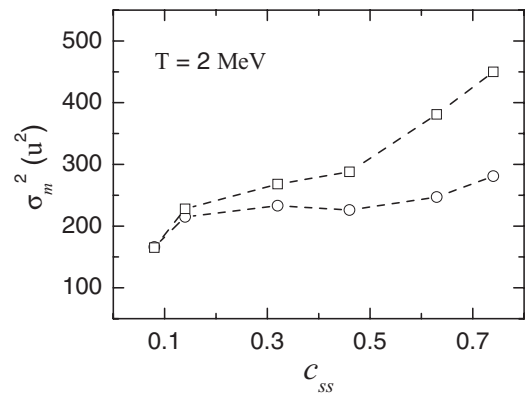

FIG. 6. The variance of the fission fragment mass distribution (σ_m^2) at the saddle ridge (empty squares) and on the scission line (empty circles) as a function of the saddle-to-scission distance obtained from dynamical model calculations without the γ^{asym} term. Lines are drawn to guide the eyes.
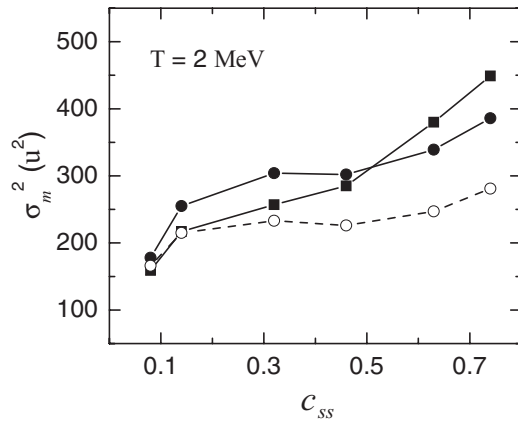
FIG. 7. The mass variances σ_m^2 calculated with (filled symbols) and without (empty symbols) the γ^{asym} term for different systems. The circles represent the variances at scission while the squares represent the variances at the saddle. The variances at the saddle for both cases (with and without γ^{asym}) are nearly the same and are indistinguishable in the plot. Lines are drawn to guide the eyes.

addition to the asymmetry distribution due to the last crossing of the saddle ridge by the fission trajectories, we also obtain the mass asymmetry distribution along the saddle ridge for the following cases. First, we calculate the asymmetry distribution by considering only those asymmetry coordinates which correspond to the first crossing of the saddle ridge by the fission trajectories. Keeping track of all the successive crossings of the saddle ridge by a fission trajectory, we further calculate the asymmetry distribution by considering the asymmetry coordinates of all such crossings. The corresponding mass variances are given for different systems as a function of c_{SS} in Fig. 9. The variances for first and last crossings are found to be very close for small values of c_{SS} while the last crossing values are larger at large c_{SS}. We interpret this observation as follows. In a stochastic process such as nuclear fission, a fission trajectory can return to a more compact shape even after it crosses the saddle ridge due to the presence of the
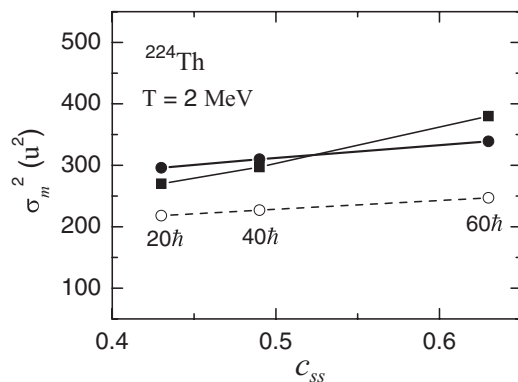

FIG. 8. The mass variances σ_m^2 calculated with (filled symbols) and without (empty symbols) the γ^{asym} term for ^{224}Th at different spins. The circles represent the variances at scission while the squares represent the variances at the saddle. The variances at the saddle for both cases (with and without γ^{asym}) are nearly the same and are indistinguishable in the plot. Lines are drawn to guide the eyes.
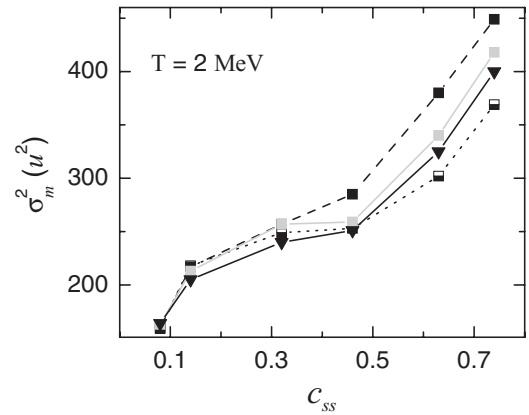

FIG. 9. The mass variances σ_m^2 corresponding to the first crossing (half-filled square), the last crossing (filled square), and all crossings (gray squares) of the saddle ridge by fission trajectories for different systems. The statistical model predictions are shown by downward triangles. Lines are drawn to guide the eyes.

random forces in the equations of motion. This backstreaming is typical of Brownian motion and has been noted earlier by several authors [31,35,50,51]. In the present analysis of two-dimensional fission dynamics, the scope of to-and-fro motion is highly restricted when the saddle ridge and the scission line are very close together (small c_{SS}). The first and last crossing points of the saddle ridge practically coincide in such cases, giving rise to almost similar distributions. For systems with larger saddle-to-scission separations, however, a larger phase space is available for to-and-fro motion in the saddle region. A fission trajectory therefore experiences the random force for a longer time interval between the first and last crossing of the saddle ridge. Consequently, the system develops higher asymmetry during its evolution from the first crossing to the last crossing of the saddle ridge. We may point out here that the subsequent change in the mass variance of the system as it moves from the saddle to the scission point has already been given earlier in Fig. 7.

We next observe in Fig. 9 that the variances of distributions considering all crossings lie in between the variances from first and last crossings, as one would expect. The asymmetry distribution obtained from all crossings of the saddle ridge by fission trajectories also corresponds to the average distribution of fission trajectories over the saddle ridge. This distribution is therefore comparable with the predictions of the statistical model. According to the statistical model [31,52], the yield of fragments with mass asymmetry α' is given as

$$Y(\alpha') = N \exp\left[-U(\alpha')/T\right], \qquad (8)$$

where $U(\alpha')$ is the potential profile along the saddle ridge and N is a normalization constant. The mass variances according to the statistical model are directly obtained from Eq. (8) and are given in Fig. 9. The variances of average distributions from the dynamical model are found to be very close to the statistical model predictions. This indicates that statistical equilibrium is almost reached in the saddle region in dynamical calculations. We next compare the mass distributions calculated at scission by the statistical and dynamical models. The statistical model values are obtained from a yield distribution as given by
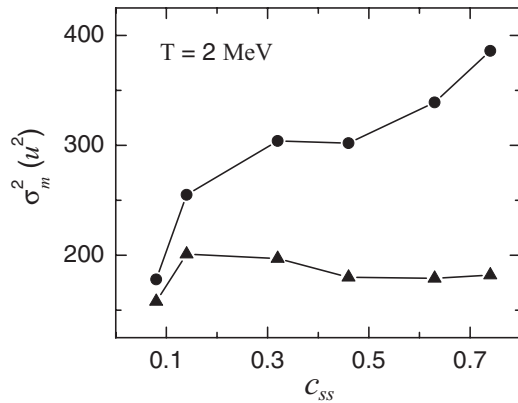
FIG. 10. The mass variances σ_m^2 at scission from the statistical model (upward triangles) and the dynamical model (circles) for different systems. Lines are drawn to guide the eyes.

Eq. (8), where the potential profile along the scission line is used. The inadequacy of the statistical model in predicting the mass variance at scission was shown earlier [9,42] and it is further illustrated here in Fig. 10. The statistical model substantially underestimates the mass variance at scission.

IV. SUMMARY AND DISCUSSION

In the preceding sections, we have studied the growth in shape asymmetry of a fissioning nucleus as it evolves from the ground state to the scission configuration. A number of systems spanning a broad range of saddle-to-scission distances have been considered for this purpose. In particular, the role of the dissipative resistance to change the mass asymmetry degree of freedom (γ^{asym}) during saddle-to-scission transition has been investigated. By comparing the asymmetry coordinate distributions at saddle and scission, it has been shown that while the conservative force guides a CN toward symmetric fission, the random force associated with γ^{asym} substantially counteracts it and drives the system toward higher asymmetry during saddle-to-scission transition. This observation has been made using asymmetry distributions at saddle and scission when both are obtained from dynamical model calculations.

The role of multiple crossing of the saddle ridge by a stochastic fission trajectory in giving rise to the asymmetry coordinate distribution at the saddle has also been investigated. It has been shown that the mass variance increases between the first and the last crossing of the saddle ridge by a fission trajectory. The subsequent development in the asymmetry coordinate distribution as the system approaches scission takes place in a manner as given in the above.

We have also examined the validity of the statistical model in the context of fission fragment mass distribution by comparing the statistical model predictions at the saddle with dynamical model results. It has been shown that the average distribution of fission trajectories over the saddle ridge obtained from the dynamical model closely follows the statistical model predictions.

At the end, we point out that the observed near cancellation of the effects due to conservative and random forces during the descent of a CN from saddle to scission in determining the fission fragment mass distribution is specific to the collective fission coordinates and the nature of dissipation used in the present work. Questions may naturally arise regarding the consequences of including more collective degrees of freedom or changing the nature of dissipation on the saddle-to-scission dynamics and the resulting fission fragment mass distribution. It was shown earlier [15] that inclusion of the neck degree of freedom substantially increases the most probable fission path from saddle to scission. Consequently, one may expect that a fission trajectory will be subjected to random forces for a longer period, giving rise to a larger mass dispersion. The saddle-to-scission dynamics also changes when one considers a non-Markovian dissipation (and random force) instead of the Markovian dissipation used in the present work. By considering non-Markovian stochastic dynamics of fission, it has been shown [53] that the mean descent time from saddle to scission increases with the relaxation time of the collective coordinates. Thus the introduction of non-Markovian features in stochastic fission dynamics is also expected to increase the fission fragment mass variance. Evidently, more calculations are needed to explore the role of saddle-to-scission descent under different stochastic dynamical models in giving rise to the fission fragment mass distribution.

[1] P. Fong, Phys. Rev. **102**, 434 (1956); Phys. Rev. Lett. **11**, 375 (1963) ; Phys. Rev. C **10**, 1122 (1974).

[2] J. R. Nix and W. J. Swiatecki, Nucl. Phys. **71**, 1 (1965).

[3] F. Plasil, D. S. Burnett, H. C. Breit, and S. G. Thompson, Phys. Rev. **142**, 696 (1966).

[4] K. T. R. Davies, A. J. Sierk, and J. R. Nix, Phys. Rev. C **13**, 2385 (1976).

[5] K. T. R. Davies, R. A. Managan, J. R. Nix, and A. J. Sierk, Phys. Rev. C **16**, 1890 (1977).

[6] G. D. Adeev and V. V. Pashkevich, Nucl. Phys. A **502**, 405c (1989).

[7] Y. Abe, S. Ayik, P.-G. Reinhard, and E. Suraud, Phys. Rep. **275**, 49 (1996).

[8] D. V. Vanin, G. I. Kosenko, and G. D. Adeev, Phys. Rev. C **59**, 2114 (1999).

[9] I. I. Gontchar, A. E. Gettinger, L. V. Guryan, and W. Wagner, Phys. At. Nucl. **63**, 1688 (2000).

[10] A. V. Karpov, P. N. Nadtochy, D. V. Vanin, and G. D. Adeev, Phys. Rev. C **63**, 054610 (2001).

[11] P. N. Nadtochy, G. D. Adeev, and A. V. Karpov, Phys. Rev. C **65**, 064615 (2002).

[12] E. G. Ryabov, A. V. Karpov, and G. D. Adeev, Nucl. Phys. A **765**, 39 (2006).

[13] P. N. Nadtochy and G. D. Adeev, Phys. Rev. C **72**, 054608 (2005).

[14] M. V. Borunov, P. N. Nadtochy, and G. D. Adeev, Nucl. Phys. A **799**, 56 (2008)

[15] S. Pal, G. Chaudhuri, and J. Sadhukhan, Nucl. Phys. A **808**, 1 (2008).

[16] H. A. Kramers, Physica (Amsterdam) **7**, 284 (1940).

[17] P. Grange, Nucl. Phys. A **428**, 37c (1984).
[18] P. Grange, J.-Q. Li, and H. A. Weidenmüller, Phys. Rev. C **27**, 2063 (1983).
[19] P. Grange, H. C. Pauli, and H. A. Weidenmüller, Phys. Lett. B **88**, 9 (1979).
[20] P. Grange and H. A. Weidenmüller, Phys. Lett. B **96**, 26 (1980).
[21] K. H. Bhatt, P. Grange, and B. Hiller, Phys. Rev. C **33**, 954 (1986).
[22] J. R. Nix, A. J. Sierk, H. Hofmann, F. Scheuter, and D. Vautherin, Nucl. Phys. A **424**, 239 (1984).
[23] F. Scheuter and H. Hofmann, Nucl. Phys. A **394**, 477 (1983).
[24] B. Jurado, K.-H. Schmidt, and J. Benlliure, Phys. Lett. B **553**, 186 (2003).
[25] B. Jurado, C. Schmitt, K.-H. Schmidt, J. Benlliure, and A. R. Junghans, Nucl. Phys. A **747**, 14 (2005).
[26] H. Hofmann, Phys. Lett. B **122**, 117 (1983).
[27] Y. Abe, C. Gregoire, and H. Delagrange, J. Phys. (Paris), Colloq. **47**, C4-329 (1986).
[28] P. Fröbrich and I. I. Gontchar, Phys. Rep. **292**, 131 (1998).
[29] D. Boilley, E. Surad, Y. Abe, and S. Ayik, Nucl. Phys. A **556**, 67 (1993).
[30] N. D. Mavlitov, P. Fröbrich, and I. I. Gontchar, Z. Phys. A **342**, 195 (1992).
[31] I. I. Gontchar and P. Fröbrich, Nucl. Phys. A **551**, 495 (1993).
[32] S. G. McCalla and J. P. Lestone, Phys. Rev. Lett. **101**, 032702 (2008).
[33] G.-R. Tillack, Phys. Lett. B **278**, 403 (1992).
[34] P. N. Nadtochy, A. Kelic, and K.-H. Schmidt, Phys. Rev. C **75**, 064614 (2007).
[35] G. Chaudhuri and S. Pal, Phys. Rev. C **63**, 064603 (2001).
[36] P. Fröbrich, I. I. Gontchar, and N. D. Mavlitov, Nucl. Phys. A **556**, 281 (1993).
[37] A. V. Karpov, P. N. Nadtochy, E. G. Ryabov, and G. D. Adeev, J. Phys. G **29**, 2365 (2003).
[38] W. Ye, Phys. Rev. C **79**, 031601(R) (2009).
[39] W. Ye, Phys. Rev. C **81**, 011603(R) (2010).
[40] G. Chaudhuri and S. Pal, Phys. Rev. C **65**, 054612 (2002).
[41] G. Chaudhuri and S. Pal, Eur. Phys. J. A **18**, 9 (2003).
[42] E. G. Ryabov, A. V. Karpov, P. N. Nadtochy, and G. D. Adeev, Phys. Rev. C **78**, 044614 (2008).
[43] T. Wada, Y. Abe, and N. Carjan, Phys. Rev. Lett. **70**, 3538 (1993).
[44] A. V. Ignatyuk, M. G. Itkis, V. N. Okolovich, G. N. Smirenkin, and A. Tishin, Sov. J. Nucl. Phys. **21**, 612 (1975).
[45] K. T. R. Davies, A. J. Sierk, and J. R. Nix, Phys. Rev. C **13**, 2385 (1976).
[46] A. J. Sierk, Phys. Rev. C **33**, 2039 (1986).
[47] J. Blocki, Y. Boneh, J. R. Nix, J. Randrup, M. Robel, A. J. Sierk, and W. J. Swiatecki, Ann. Phys. (NY) **113**, 330 (1978).
[48] A. J. Sierk and J. R. Nix, Phys. Rev. C **21**, 982 (1980).
[49] J. Randrup and W. J. Swiatecki, Nucl. Phys. A **429**, 105 (1984).
[50] J.-D. Bao and Y. Jia, Phys. Rev. C **69**, 027602 (2004).
[51] J. Sadhukhan and S. Pal, Phys. Rev. C **79**, 064606 (2009).
[52] A. Ya. Rusanov, V. V. Pashkevich, and M. G. Itkis, Phys. At. Nucl. **62**, 547 (1999).
[53] V. M. Kolomietz and S. V. Radionov, Phys. Rev. C **80**, 024308 (2009).